Supplemental Material: Critical properties of the measurement-induced transition in random quantum circuits

Aidan Zabalo,[1] Michael J. Gullans,[2] Justin H. Wilson,[1] Sarang Gopalakrishnan,[3] David A. Huse,[2,4] and J. H. Pixley[1]

[1] *Department of Physics and Astronomy, Center for Materials Theory, Rutgers University, Piscataway, NJ 08854 USA*
[2] *Physics Department, Princeton University, Princeton, New Jersey 08544, USA*
[3] *Department of Engineering Science and Physics, CUNY College of Staten Island, Staten Island, New York 10314, USA and Initiative for the Theoretical Sciences, CUNY Graduate Center, New York, New York 10016 USA*
[4] *Institute for Advanced Study, Princeton, New Jersey 08540, USA*

NUMERICAL METHODS

When calculating quantities such as the bipartite entanglement entropy, bipartite mutual information, or tripartite mutual information, there is an even-odd effect that occurs depending on whether or not there is a gate across the location of the cut. To deal with these effects we use the following prescription when calculating a quantity Q:

1. Perform a layer of gates on sites [1,2], [3,4], ...
2. Calculate quantity $Q^{(1)}$
3. Perform a layer of measurements
4. Perform a layer of gates on sites [2,3], [4,5], ...
5. Calculate quantity $Q^{(2)}$
6. Average results: $Q = \frac{1}{2}\left(Q^{(1)} + Q^{(2)}\right)$

RÉNYI INDEX N = 0

The quantities with Rényi index $n = 0$ are difficult to calculate numerically since all eigenvalues must be raised to the zeroth power in the sum. One is then forced to introduce a cutoff to prevent arbitrarily small eigenvalues from contributing to the sum. This poses significant difficulties for estimating p_c from the tripartite mutual information, $\mathcal{I}_{3,n=0}$, as shown by its sensitivity to the cutoff in Fig. S1. Choosing the cutoff to be machine epsilon for the binary64 number format, $\approx 2.22 \cdot 10^{-16}$, the critical values are estimated to be $p_c = 0.45(3)$ and $\nu = 1.5(3)$ as shown shown in Fig. S2. The estimated values are different than the exact values, $p_c = 0.5$ and $\nu = 4/3$, given by the 2-D percolation mapping.

RÉNYI INDEX N $\geq$ 1

The data for the Rényi indices $n \gtrsim 0.1$ do not suffer from the numerical accuracy issues described in the previous section. This allows for the determination of an accurate value for the critical measurement rate, p_c. The main paper contains the results of the TMI and the data collapse from a finite size scaling analysis for $n = 1$. In Fig. S3, the other Rényi's ($n = 2, 5, \infty$) are shown to have similar quality of data and collapse.

DATA COLLAPSE

In order to determine the critical measurement rate, p_c, and the critical exponent, ν, we perform a finite size scaling analysis based on the procedure outlined by Kawashima and Ito [1]. In summary, if we assume $\mathcal{I}_{3,n} = F\left[(p - p_c)L^{1/\nu}\right]$ for some arbitrary scaling function F, then we expect the data for different system sizes to collapse on each other for the appropriate choices of p_c and ν when plotting $y = \mathcal{I}_{3,n}$ vs $x = (p - p_c)L^{1/\nu}$.

To judge the quality of collapse we study the objective function $O(p_c, \nu)$ defined as,

$$O(p_c,\nu) \equiv \frac{1}{n-2}\sum_{i=2}^{n-1} w(x_i, y_i, d_i \mid x_{i-1}, y_{i-1}, d_{i-1}, x_{i+1}, y_{i+1}, d_{i+1}), \tag{S1}$$

where $x_i = (p_i - p_c)L_i^{1/\nu}$, $y_i = \mathcal{I}_{3,n,i}$, and $d_i = \sigma_{y_i}$ are the scaled data sorted such that $x_1 < x_2 < ... < x_n$. The quantity $w(x, y, d \mid x', y', d', x'', y'', d'')$ is defined as

$$w \equiv \left(\frac{y-\bar{y}}{\Delta(y-\bar{y})}\right)^2 \tag{S2}$$

$$\bar{y} \equiv \frac{(x''-x)y' - (x'-x)y''}{x''-x'} \tag{S3}$$

$$[\Delta(y-\bar{y})]^2 \equiv d^2 + \left(\frac{x''-x}{x''-x'}d'\right)^2 + \left(\frac{x'-x}{x''-x'}d''\right)^2. \tag{S4}$$

Minimizing Eq. S1 corresponds to minimizing the deviation of each point (x_i, y_i) from the line determined by its adjacent points (x_{i-1}, y_{i-1}) and (x_{i+1}, y_{i+1}). For an ideal collapse, $O(p_c, \nu)$ attains its minimum value = 1.

For a given dataset, the value of Eq. S1 can be plotted for different values of p_c and ν as shown in Fig. S4. The estimate of the critical values is given by the location of the global minimum: (p_c^*, ν^*). To estimate the error in the values p_c^* and ν^*, a region around the minimum value is taken such that $O(p_c, \nu) \leq 1.3 \cdot O(p_c^*, \nu^*)$, shown as the white contour. Repeating the procedure for the different Rényi indices results in the critical values shown in Fig. S5.

BIPARTITE MUTUAL INFORMATION

The bipartite mutual information, $\mathcal{I}_{2,n=1}$, between antipodal regions of size $L/4$ contains a crossing at p_c but suffers from stronger finite size drifts than $\mathcal{I}_{3,n=1}$ as shown in Fig. S6. This is consistent with the behavior seen in the stabilizer circuit when compared out to larger sizes up to $L = 512$.

DYNAMICAL EXPONENT z

To determine the dynamical exponent, z, we construct a circuit with periodic boundary conditions starting from an entangled Haar state such that an ancilla is maximally entangled with a qubit in the spin chain. We fix the measurement rate $p = p_c = 0.17$ and calculate the entanglement entropy decay of the ancilla as a function of time as shown in Fig. S7. The entanglement entropy should scale as $S(t, L) \sim F(t/L^z)$ for an arbitrary scaling function F. From data collapse of system sizes $L = 12, 16, 20$, we find $z = 1.06(4)$ which is close to the value of $z = 1$ for conformal invariance [2, 3].

ORDER PARAMETER

An order parameter can be defined for the transition by introducing a reference qubit that is maximally entangled with a single site in the system and calculating its entanglement entropy. In Fig. S8 a crossing at similar values of p_c is observed for the Rényi indices (a) $n = 0.3$ and (b) $n = 1$ indicating that all $n > 0$ are described by the same transition.

CORRELATION FUNCTION

The correlation function $C(t - t_0) = I_1(\tilde{A}, \tilde{B}) = S_1(\tilde{A}) + S_1(\tilde{B}) - S_1(\tilde{A} \cup \tilde{B})$ is defined as the mutual information between two ancilla qubits entangled with the system at time t_0. The correlation function obeys the critical finite-size scaling form $C(t - t_0) \sim L^{-\eta} g((t - t_0)/L)$, where the exponent η depends on the different boundary conditions.

In the case of our numerical simulations we define the bulk exponent η from the circuit with periodic boundary conditions starting from a product state. The circuit is run to a time $t_0 = 2L$ and the ancillas are maximally

entangled with antipodal spins. This corresponds to a two-point order parameter correlation function on a cylinder with complex coordinates for the two ancilla $(z_1', z_2') = (0, iL/2)$, which can be related to standard correlation functions in the complex plane through the conformal mapping $z = e^{2\pi z'/L}$.

In Fig. S9, we show how the surface exponents are related to different correlation functions in the random circuit geometry with open boundary conditions. Here, $\phi_{A/B/C}(b)$ denotes the order parameter operator at scale b. The scaling dimension in the bulk is $\eta/2$, the scaling dimension at the surface is $\eta_\parallel/2$, and the scaling dimension for two-point functions between the surface and bulk is given by $\eta_\perp$ that satisfies the scaling relation $2\eta_\perp = \eta + \eta_\parallel$ [4, 5]. In the random circuit geometry, the surface exponent $\eta_\parallel$ is given by a circuit with open boundary conditions starting from a product state. The circuit is run to a time $t_0 = 2L$ and the ancillas are maximally entangled with the edge spins so that $(z_1', z_2') = (0, iL)$. Another estimate of $\eta_\parallel$ is given by a circuit with periodic boundary conditions starting from a product state where at time $t_0 = 0$ an ancilla is maximally entangled with a spin in the system. The latter has non-universal early time dynamics that make it difficult extract $\eta_\parallel$. The surface exponent $\eta_\perp$ is given by a circuit with open boundary conditions starting from a product state. The circuit is run to a time $t_0 = 2L$ and the ancillas are maximally entangled with the edge and middle spins so that $(z_1', z_2') = (0, iL/2)$.

The main text contains results for η and $\eta_\parallel$ for the Rényi index $n = 1$. For an arbitrary value of the Rényi index we can define the correlation function as $C_n(t - t_0) = I_n(\tilde{A}, \tilde{B}) = S_n(\tilde{A}) + S_n(\tilde{B}) - S_n(\tilde{A} \cup \tilde{B})$. In Figs. S10 and S11 the other Rényi's ($n = 2, 5, \infty$) are shown to have similar quality of data and collapse. In Fig. S12 we show results for the alternate estimate of $\eta_\parallel$ where we find values different than those reported in the main text, however, we find the values from the main text hold reasonably well at late times where the dynamics are expected to be universal. Fig. S13 also shows results for $\eta_\perp$ for $n = 1, 2, \infty$.

ORDER PARAMETER DYNAMICS

In Fig. S14, we show the dynamics of the order parameter S_Q^1 for the case of the Clifford and Haar gate models at their respective critical measurement rates for $L = 12$. Here, S_Q^1 is the entropy of the reference qubit averaged over measurement outcomes (trajectories) for a fixed realization of the circuit and measurement locations. The initial state was chosen to be a pseudo-random stabilizer/Haar random state of the system and reference. The pseudo-random stabilizer state was generated by running a depth $2L$ circuit without measurements on an initial product stabilizer state. In the case of the stabilizer circuits, the purification of the reference qubit happens instantaneously in a single measurement. The universal decay curve with time only arises after averaging over random choices of gates or measurement locations. For the Haar random circuit, in contrast, the randomness in the measurement outcomes is sufficient to lead to a nontrivial decay for the order parameter. This is an important qualitative distinction in the critical dynamics between these two models. In the case of the stabilizer circuit, the order parameter dynamics are not self-averaging even in the thermodynamic limit, whereas the intrinsic randomness of the measurement outcomes is enough to lead to (at least partial) self-averaging behavior for the Haar model.

Another interesting observation is that S_Q^1 is monotonically decreasing with time in both cases. Using the relation between S_Q^1 and the mutual information between the reference qubit and an effective environment associated with the measurement outcomes [6–8], such a monotonic decay implies that, for these circuits, the information about the state of the reference qubit flows irreversibly into the environment. This trend is consistent with the fact that the unitary-projective measurement dynamics effectively samples the quantum trajectories of a system interacting with a perfect Markovian environment.

MINIMAL-CUT PICTURE FOR MUTUAL INFORMATION

In this section we briefly discuss the behavior of the bipartite and tripartite mutual information, $\mathcal{I}_{2,n}$ and $\mathcal{I}_{3,n}$, within the minimal cut picture. For Haar-random circuits, the minimal cut picture is exact for $n = 0$, regardless of the local Hilbert-space dimension; within the minimal cut, the entanglement transition is a percolation transition. We will restrict our discussion to partitions of a system of size L, with periodic boundary conditions, into four equally sized pieces (each of length $L/4$) labeled A, B, C, D as in Fig. S15. Specifically, we will consider $\mathcal{I}_{2,0}(A : C)$ and $\mathcal{I}_{3,0}(A : B : C)$; for simplicity, in what follows we will suppress the indices and just call these quantities $\mathcal{I}_2$ and $\mathcal{I}_3$. Although our discussion is quantitative only for this specific choice of observable, we have found that the generic and percolation transitions are qualitatively similar, so our analysis offers useful guidance for the general case.

We begin with $\mathcal{I}_2 = S(A) + S(C) - S(A \cup C)$; we assume the circuit has been run out to times considerably longer than system size. The entanglement of A is given by the minimal number of bonds that must be crossed by a polymer

beginning and ending at endpoints of A. For the disjoint region $A \cup C$, one has two ways to connect the polymers (Fig. S15a), A_1A_2, C_1C_2 and A_2C_1, C_2A_1; the minimal cut is the shorter of these. In the absence of measurements, the two arrangements cut the same number of bonds, so $\mathcal{I}_2 = 0$. Measurements locally cut bonds; thus, for nonzero measurement probability, in a given realization of the circuit, the two minimal-cut arrangements pass through different numbers of cut bonds. In half the realizations, the minimal cut for $A \cup C$ is the union of those for A and C, and $\mathcal{I}_2 = 0$; in the other half, there is nonzero $\mathcal{I}_2$. Following a standard analysis of polymers in random media [9] we find that the typical scale of fluctuations between the two minimal cuts, and therefore the mutual information in the volume law phase, scales as $\sim L^{1/3}$. This latter prediction is consistent with the data on Haar circuits (Fig. S16); moreover, the minimal-cut prediction that some nonvanishing fraction of the samples have zero mutual information in the thermodynamic limit is consistent with the data on stabilizer circuits in the volume law phase, as shown in Fig. S17 (by contrast, the distribution for Haar circuits is continuous, but at the achievable sizes we cannot conclude whether there is a distinct peak near zero mutual information). Thus the minimal cut picture appears to qualitatively describe many features of the mutual information beyond the $n = 0$ limit.

In the area law phase, there is a percolating cluster of bonds that are cut because of measurements. The polymer from each end of A travels some distance into the circuit, finds the cluster of cut bonds (which we can regard as a large "void" [10]), and moves freely through it to join up with the polymer from the other end. The entanglement is set by the local geometry of getting from (say) A_1 to the void (the "boundary" sections in Fig. S15b). In the area law phase there is no contribution from the "bulk" of the region and thus no distinction between the two ways of closing the minimal cut; the mutual information is thus zero, except in instances that are exponentially rare in the region size.

The behavior at the critical point is intermediate. The polymer goes through a hierarchy of voids, each of which is larger than the previous one by some factor; to travel a distance L, therefore, requires crossing $\sim \log L$ bonds [10]. To get from A_1 to A_2 (or C_2), the polymer first makes it out of A_1 into a void of size $\sim L$, crosses that void, and then goes through increasingly small voids until it reaches A_2 (or C_2). Crucially, the optimal path to the large void is the same regardless of which way one closes the minimal cut. Therefore, the differences between the two different minimal cuts come only from the largest few scales, and are thus $O(1)$; thus $\mathcal{I}_2$ at the critical point is expected to be constant.

We now turn to $\mathcal{I}_3$, for which the analysis is similar but more involved. As noted before, we expect the local behavior near the cuts to be the same regardless of how the cuts will eventually line up; therefore we can schematically split up our entanglement cuts into "bulk" and "boundary" segments as in Fig. S15b. In $\mathcal{I}_3$, the boundary segments cancel out, leading to the formula (expressed in the notation of that figure):

$$\begin{aligned}\mathcal{I}_3 = &\min(a, b+c+d) + \min(b, a+c+d) + \min(c, a+b+d) \\ &-\{\min(a+b, c+d) + \min(a+c, b+d) + \min(a+d, b+c)\}. \end{aligned} \tag{S5}$$

In the volume law phase, a, b, c, d are all comparable and volume-law in magnitude, so $\mathcal{I}_3 \approx -2a$ is negative and volume-law. In the area law phase, by contrast, all four numbers are essentially zero (since the polymer can move through a void), so $\mathcal{I}_3 = 0$ (since the boundary contributions cancel exactly). At the critical point, the "bulk" contribution is $O(1)$, as argued above, so $\mathcal{I}_3$ is also $O(1)$.

One can see that this expression (S5) is never positive. Without loss of generality take $a \geq b \geq c \geq d$. The expression then simplifies to $\mathcal{I}_3 = \min(a, b+c+d) - \min(a+d, b+c) - d$. There are two cases: (i) $b+c \geq a+d$, in which case $\mathcal{I}_3 = a - (a+d) - d = -2d \leq 0$; and (ii) $a+d > b+c$, in which case $\mathcal{I}_3 = \min(a, b+c+d) - (b+c+d) \leq 0$. This establishes that $\mathcal{I}_3 \leq 0$ within the minimal cut picture; together with our previous argument that it should be $O(1)$ in magnitude, we conclude that $\mathcal{I}_3$ should be a negative number of order unity at the transition. This appears to be the case not just for percolation, as derived above, but also for Haar and stabilizer circuits.

[1] N. Kawashima and N. Ito, J. Phys. Soc. Jpn. **62**, 435 (1993).
[2] C.-M. Jian, Y.-Z. You, R. Vasseur, and A. W. W. Ludwig, "Measurement-induced criticality in random quantum circuits," (2019), arXiv:1908.08051.
[3] Y. Li, X. Chen, and M. P. A. Fisher, Phys. Rev. B **100**, 134306 (2019).
[4] K. Binder, *Phase Transitions and Critical Phenomena* vol. 8, ed. C. Domb and J. L. Lebowitz (New York: Academic) (1983).
[5] J. L. Cardy, Nucl. Phys. B **240**, 514 (1984).

[6] M. J. Gullans and D. A. Huse, (2019), arXiv:1910.00020.
[7] M. J. Gullans and D. A. Huse, (2019), arXiv:1905.05195.
[8] S. Choi, Y. Bao, X.-L. Qi, and E. Altman, (2019), arXiv:1903.05124.
[9] M. Kardar and Y.-C. Zhang, Phys. Rev. Lett. **58**, 2087 (1987).
[10] B. Skinner, J. Ruhman, and A. Nahum, Phys. Rev. X **9**, 031009 (2019).

SUPPLEMENTAL FIGURES

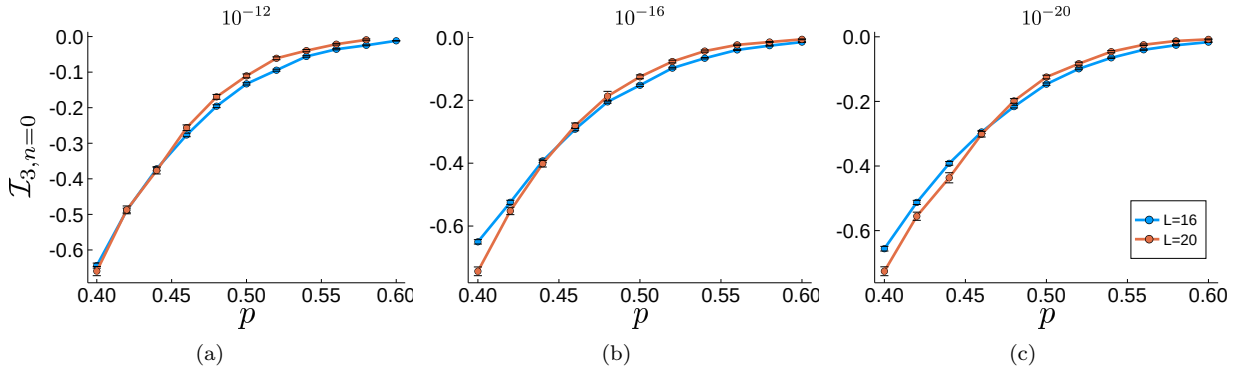

FIG. S1. *Sensitivity to cutoff.* The Rényi index $n = 0$ raises all eigenvalues to the zeroth power and it is necessary to introduce a cutoff to prevent arbitrarily small eigenvalues from contributing to the sum. For a fixed set of system sizes, the crossing in $\mathcal{I}_{3,n=0}$ drifts towards a larger p_c as the cutoff is increased. This leads to large errors when estimating p_c and ν.

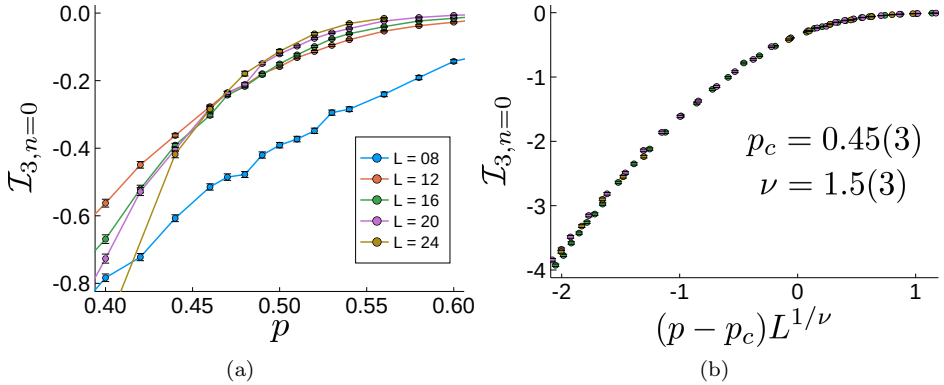

FIG. S2. *Rényi index $n = 0$ tripartite mutual information.* The (a) tripartite mutual information and (b) data collapse for a cutoff given by machine epsilon for the binary64 number format. The estimated values of p_c and ν are slightly different than the exact value given by the 2-D percolation mapping.

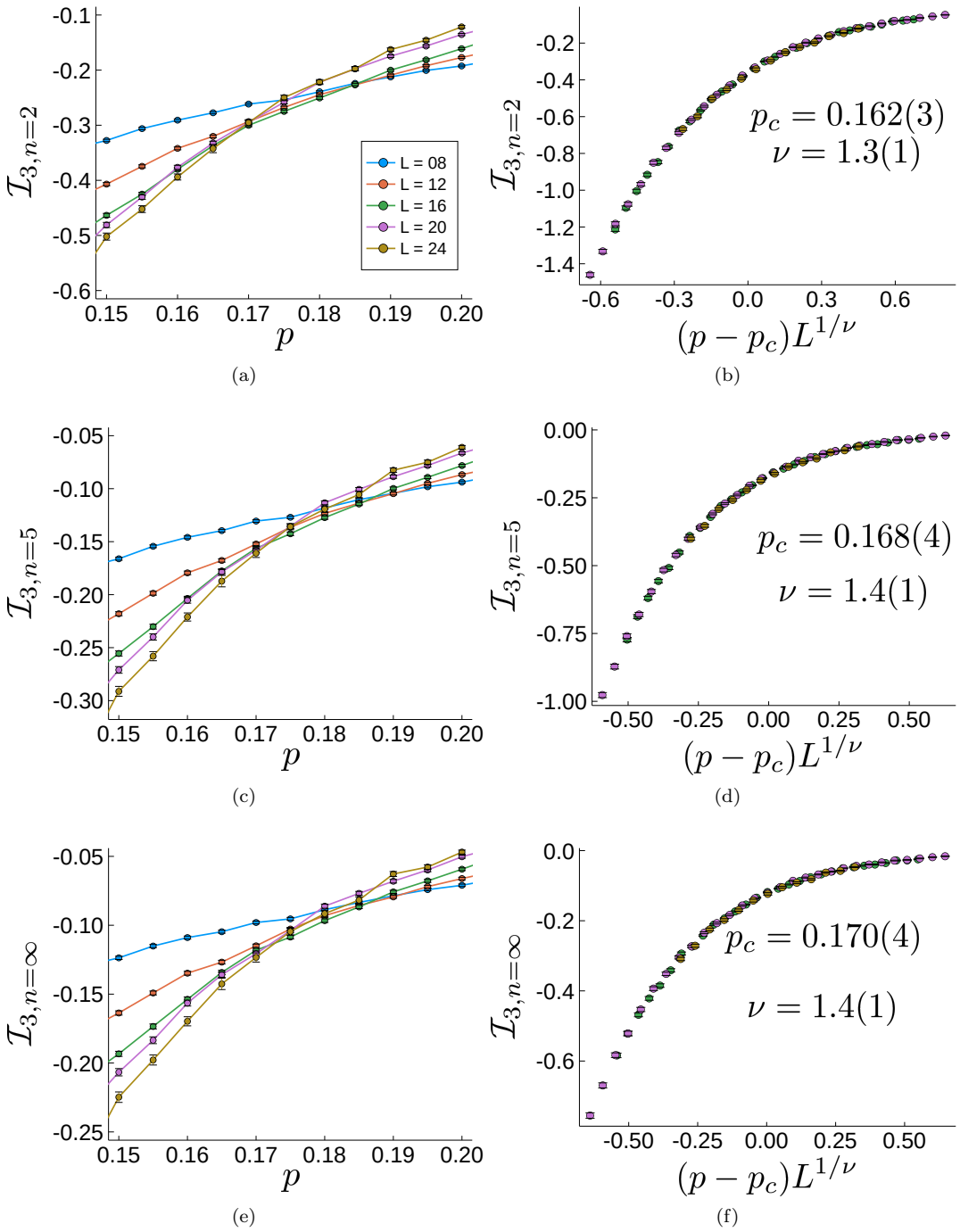

FIG. S3. *Tripartite mutual information near the transition.* The crossing of $\mathcal{I}_3$ for Rényi indices $n = 2, 5, \text{and} \infty$ is shown in (a), (c), and (e), respectively. The corresponding data collapse using the critical values determined from the finite size scaling analysis is shown in (b), (d), and (f).

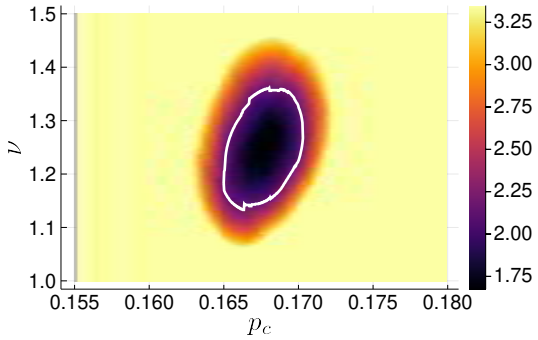

FIG. S4. *Color plot of the objective function* $O(p_c, \nu)$. The critical values are determined from the global minimum of the objective function $O(p_c, \nu)$. To estimate the error bars in the critical values we take a region (outlined in white) around the minimum value of the objective function such that $O(p_c, \nu) < 1.3 \cdot O(p_c^*, \nu^*)$.

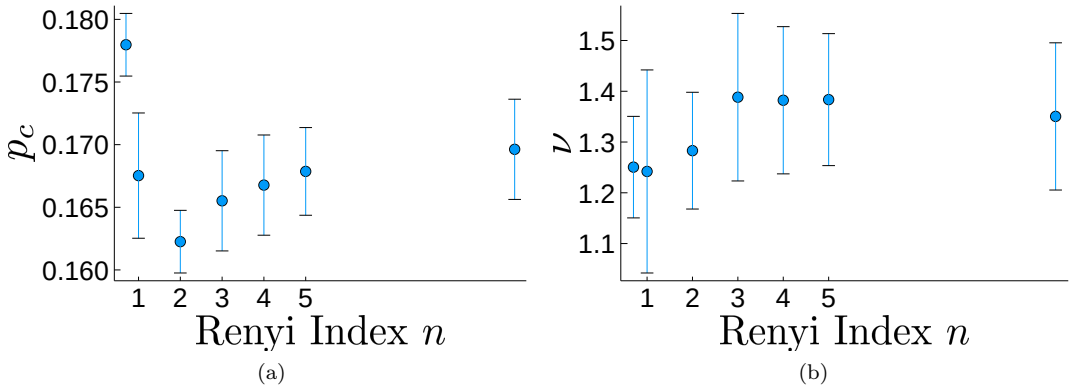

FIG. S5. *Rényi index dependence of the critical values.* The critical values p_c and ν obtained from the global minimum of the objective function $O(p_c, \nu)$. The unlabeled data point corresponds to $n \to \infty$.

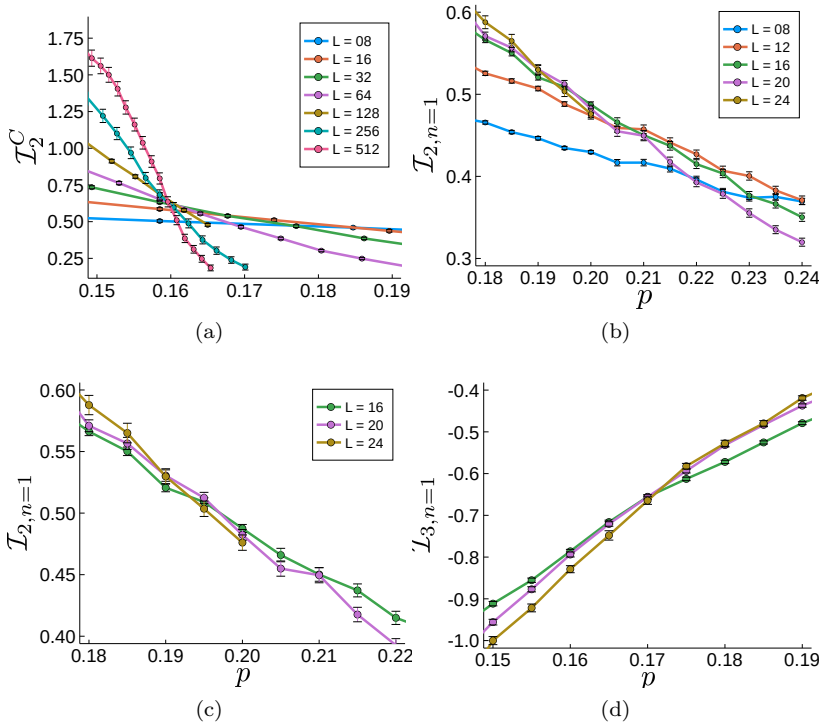

FIG. S6. *Mutual information crossing.* By studying the stabilizer circuit, (a), we find the bipartite mutual information between antipodal regions of size $L/4$ contains a crossing at p_c that drifts heavily for small system sizes. The Haar circuit shows similar finite size drifts in the bipartite mutual information, (b) and (c), that are absent in the (d) tripartite mutual information.

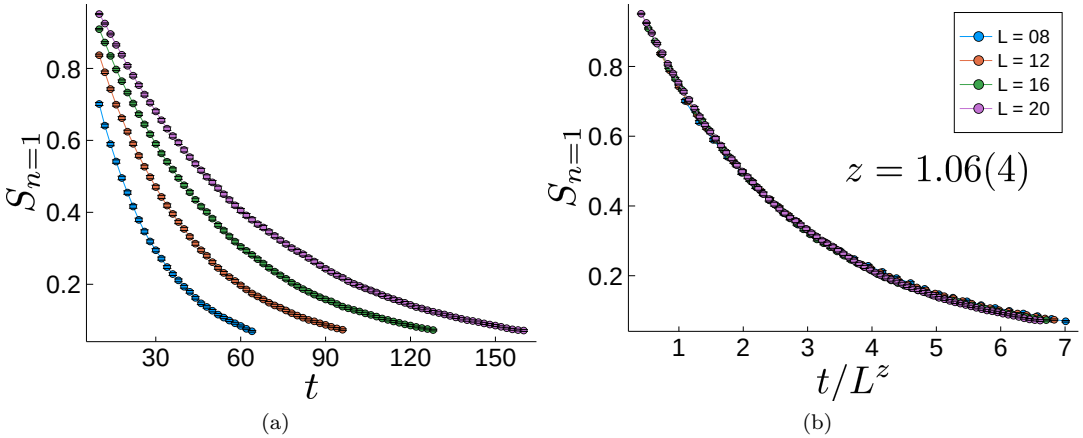

FIG. S7. *Dynamical exponent.* (a) The entanglement entropy decay as a function of time for an ancilla maximally entangled with a qubit in the circuit at $p = p_c$. (b) Through data collapse of the entanglement entropy we find the dynamical exponent $z = 1.06(4)$ which is close to the value of $z = 1$ for conformal invariance.

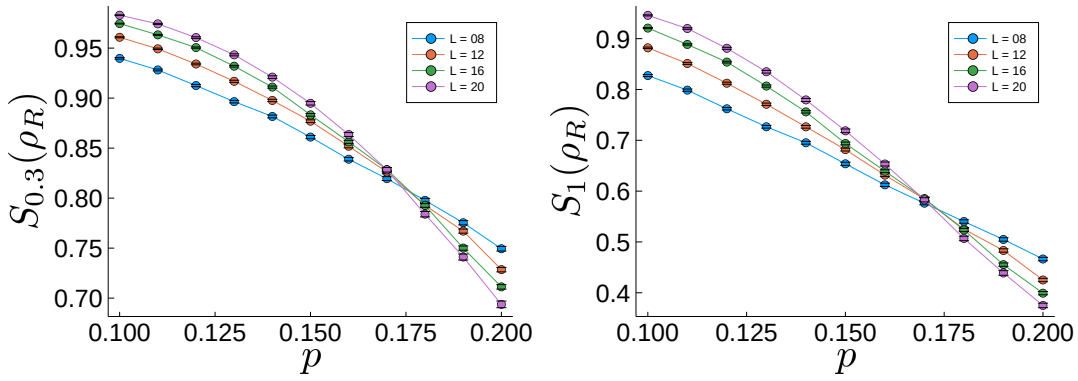

FIG. S8. *Order parameter.* The entanglement entropy of the reference qubit behaves as an order parameter for the transition. A crossing at similar p_c is observed for the Rényi indices (a) $n = 0.3$ and (b) $n = 1$ indicating that all $n > 0$ are described by the same transition.

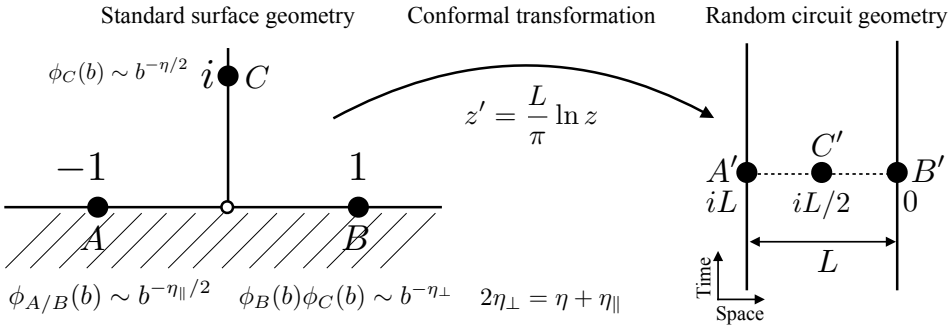

FIG. S9. *Surface exponent definition.* The standard surface geometry for defining surface exponents in a 2D system [4, 5] can be related to the geometries we consider in the random circuit through the conformal transformation $z' = (L/\pi) \ln z$. Here, $\phi_{A/B/C}(b)$ denotes the order parameter operator at scale b.

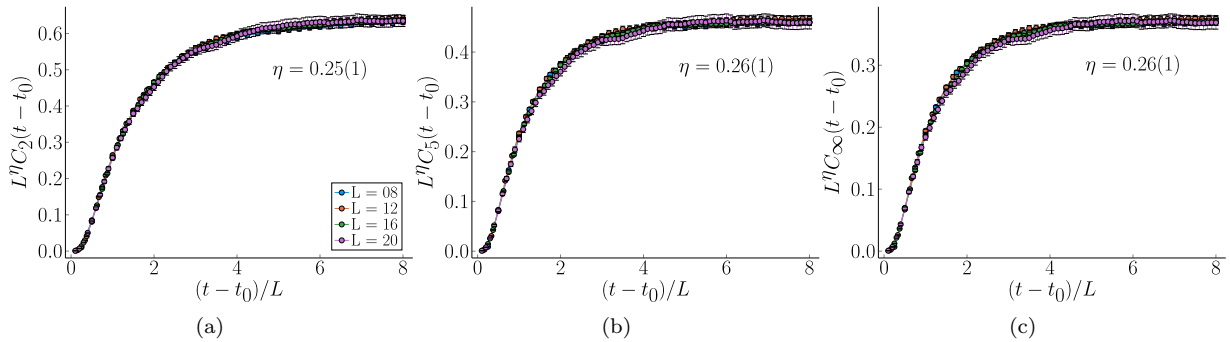

FIG. S10. *Bulk exponent η.* The bulk η is given by a circuit with periodic boundary conditions starting from a product state. The circuit is run to a time $t_0 = 2L$ and the ancillas are maximally entangled with antipodal spins.

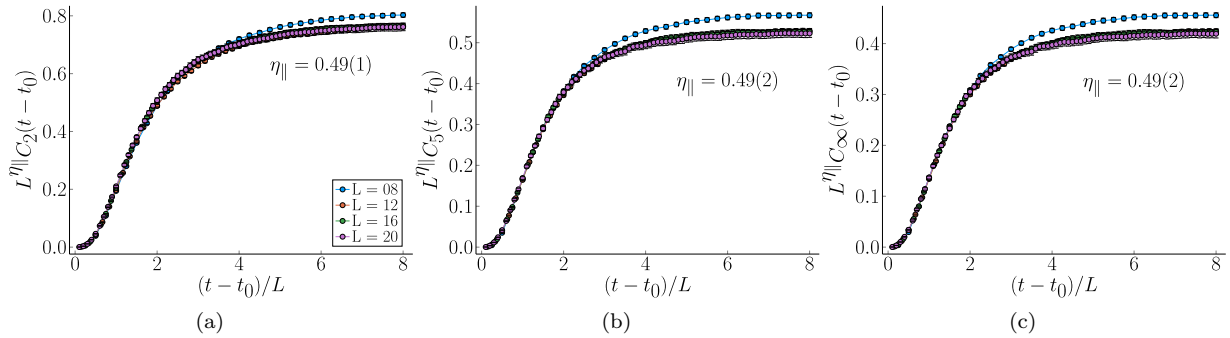

FIG. S11. *Surface exponent* $\eta_\parallel$. The surface $\eta_\parallel$ is given by a circuit with open boundary conditions starting from a product state. The circuit is run to a time $t_0 = 2L$ and the ancillas are maximally entangled with the edge spins.

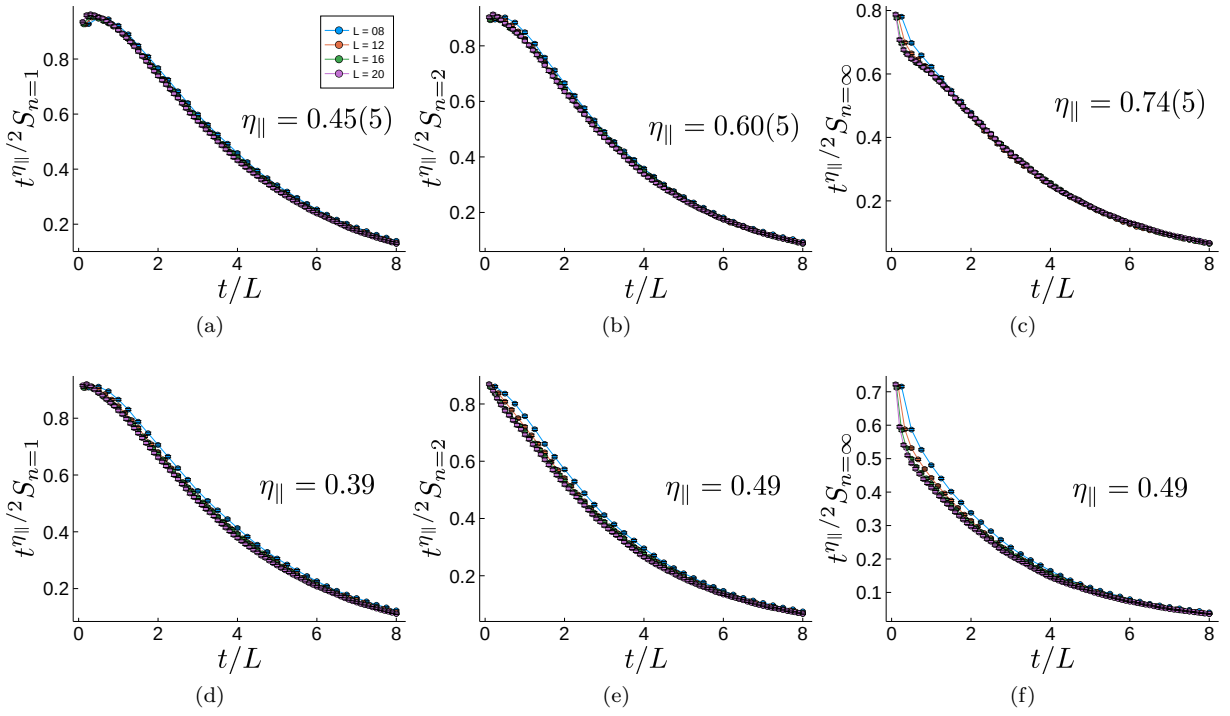

FIG. S12. *Surface exponent* $\eta_\parallel$. The surface $\eta_\parallel$ is also given by a circuit with periodic boundary conditions starting from a product state where at time $t_0 = 0$ an ancilla is placed in a maximally entangled state with a spin in the system. The collapse of the data for different Rényi indices $n = 1, 2$, and ∞ is shown in (a), (b), and (c), respectively. These results for $\eta_\parallel$ are different than the estimate used in the main text due to non-universal early time dynamics. However, at late times, the data collapses using the values of $\eta_\parallel$ from the main text, as shown in (d), (e), and (f).

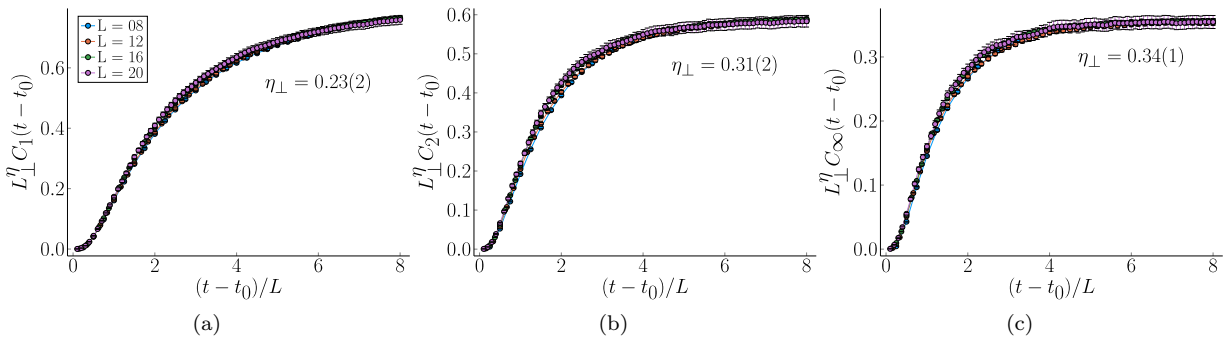

FIG. S13. *Surface exponent* $\eta_\perp$. The surface $\eta_\perp$ is given by a circuit with open boundary conditions starting from a product state. The circuit is run to a time $t_0 = 2L$ and the ancillas are maximally entangled with the edge and middle spins.

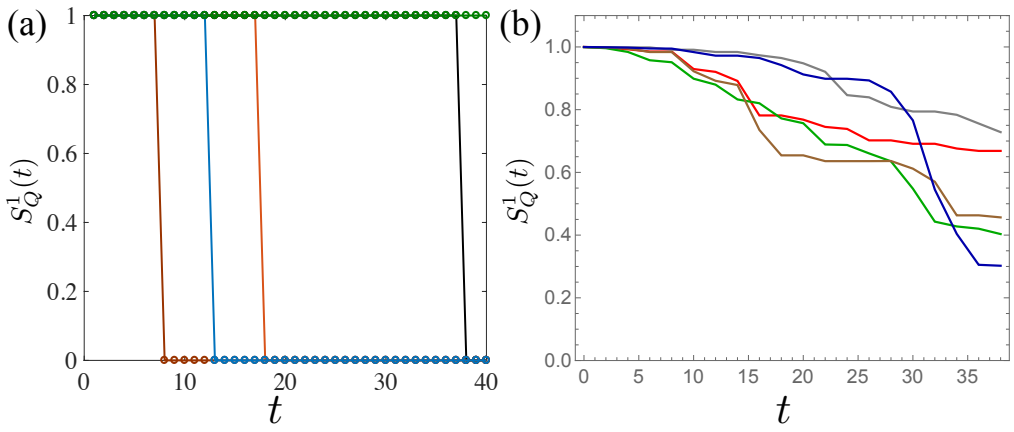

FIG. S14. *Order parameter dynamics.* For fixed gates and measurement locations we average the entropy of a single reference qubit over measurement outcomes to determine the order parameter $S_Q^1(t)$ for this circuit [6]. We took an initial state consisting of a pseudo-random stabilizer state/Haar random state between the reference and system in the case of Clifford/Haar gates. (a) Dynamics of $S_Q^1(t)$ for five different realizations of the stabilizer circuit at $p = p_c^C$. The purification of the reference occurs in a single time step at a time that depends on the choice of circuit. (b) Dynamics of $S_Q^1(t)$ for five different realizations of the Haar random circuit at $p = p_c^H$. In sharp contrast to the stabilizer circuits, the purification occurs gradually over many measurements. We took $L = 12$ in both panels and each curve in (b) is averaged over 10 000 trajectories. No such averaging is required in (a) because S_Q^1 is independent of the measurement outcomes for stabilizer circuits.

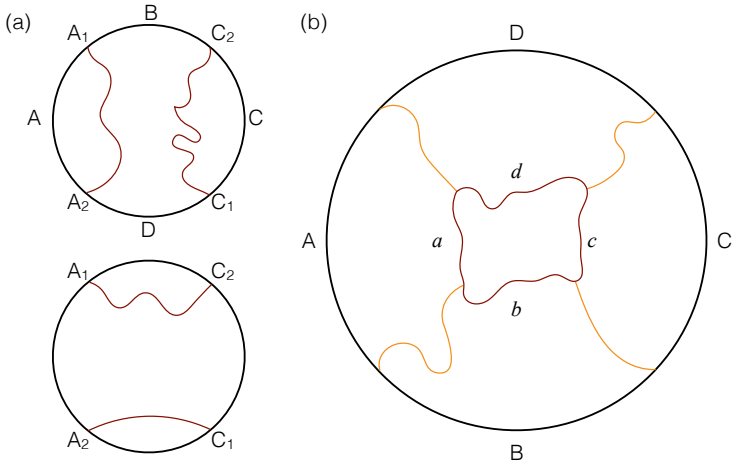

FIG. S15. *Minimal cut.* Minimal cut diagrams for partitions of a system into four equal segments. (a) Schematic minimal cut diagrams for the bipartite mutual information $\mathcal{I}_{2,0}(A:C)$. For the region $A(C)$, one requires the optimal path from A_1 to A_2 (C_1 to C_2), shown in the upper figure. However, for the region $A \cup C$ one only needs paths with endpoints at A_1, A_2, C_1, C_2; there are two of these, shown in the upper and lower figures. When the lower cut determines $S_0(A \cup C)$, the mutual information is nonzero. (b) Diagram for computing the tripartite mutual information $\mathcal{I}_3$. It is convenient to separate the minimal cuts into "boundary" parts (denoted by light orange lines) and "bulk" parts (denoted by dark red lines). In $\mathcal{I}_3$ the boundary parts cancel but the bulk parts do not.

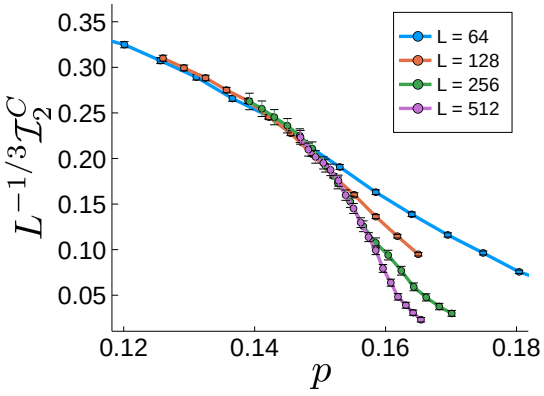

FIG. S16. *Mutual information scaling.* The mutual information in the volume-law phase for the stabilizer circuits scales as $L^{1/3}$ as expected from the minimal cut picture.

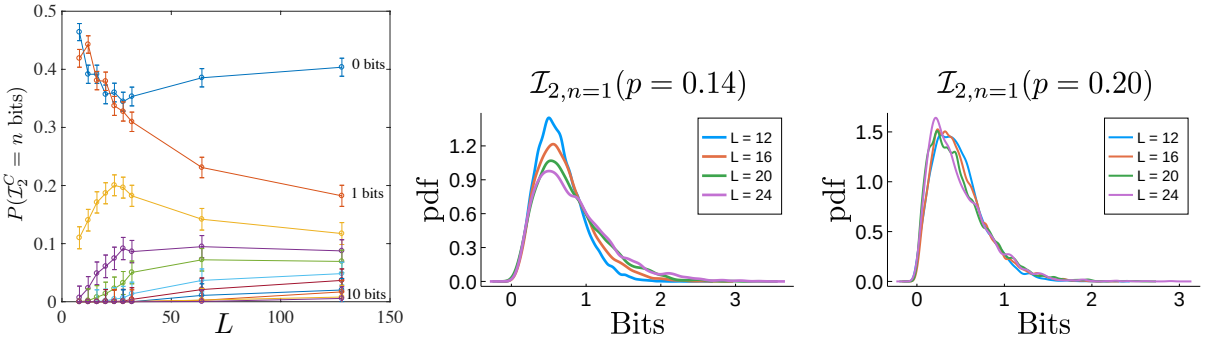

(a) (b) (c)

FIG. S17. *Mutual information probability distributions.* (a) Stabilizer circuits at $p = 0.08$, i.e., deep in the volume-law phase. Although $\mathcal{I}_2$ grows with system size, L, the probability of finding zero mutual information appears to approach a constant, as the minimal cut picture would predict. (b),(c): analogous data for Haar circuits. Unlike the stabilizer case, here $\mathcal{I}_2$ is continuously distributed.